Design and Early Age Performance of Sustainable One-Part Geopolymers for Well Cementing

Mohamed Omran[1]*, Maria Paiva[2], and Mahmoud Khalifeh[1]

[1]Department of Energy and Petroleum Engineering, University of Stavanger (UiS)
[2]Sustainable Materials Research Center (NUMATS), Federal University of Rio de Janeiro (UFRJ)

Summary

One-part geopolymers, known as "just add water" (JAW), alkali-activated formulation is presented in this work. This work reveals the design and development of short-term properties of JAW geopolymers for use in oilwell cementing and well abandonment. Granite-based mix designs normalized with a byproduct slag and a small amount of microsilica as precursors were developed. The solid activator is composed of potassium silicate and potassium hydroxide, which are mixed with the precursors to synthesize the JAW formulation. Zinc oxide is used as a strength booster admixture. The cementing properties of the developed granite-based mix designs were characterized by investigating reaction phases and mechanical properties. Dissolution, heat evolution, pumpability, strength development, and mineralogy are also studied. The results show that a positive correlation among all the given analyses for the final geopolymeric product is quite observable. Zinc oxide is favorable to be added for optimizing the given precursor mix design to enhance the solubility and leads to much higher heat evolutions. Furthermore, it develops early strength up to 16 MPa without any negative effect on the investigated one-part geopolymer slurries.

Introduction

The primary objective of all cementing operations in the oil and gas industry is the effective placement of barrier materials that can fulfill their functions at downhole conditions. After setting, the hardened cement is expected to work as a physical barrier, providing proper long-term zonal isolation within the wellbore. Additionally, safe and economical cementing operations are other important requirements and key paths to improve the overall performance of well-cementing systems (Nelson and Guillot 2006; Khalifeh and Saasen 2020).

Within this context, ordinary Portland cement (OPC) is the prime material used for zonal isolation and well abandonment for more than a century, mainly due to its worldwide manufacturing infrastructure, raw materials, known chemistry, availability, and pricing (Hewlett 2001; Nelson and Guillot 2006; Taylor 1997). Even though OPC chemistry is well-known and developed, there are technical constraints reported in the literature regarding its short- and long-term properties (Deshpande et al. 2015; Simao et al. 2016). OPC durability limitations are even more challenging to overcome when considering the harsh conditions present in the oil and gas wells environment (Bergen et al. 2022; Kiran et al. 2017; Nelson and Guillot 2006). Moreover, its production contributes up to 8% of the global CO_2 emissions (Andrew 2019), from the decomposition of carbonates and high fossil fuel consumption. Altogether, these aspects represent a powerful driving force toward the development of cementitious materials with lower carbon footprint to achieve global carbon dioxide reduction goals (Damtoft et al. 2008; IEA 2021).

Geopolymers are a subcategory of alkali-activated based materials (Davidovits 2008; Palomo et al. 2014), which have been estimated to have between 70% and 80% lower CO_2 emissions per ton of produced material (Flatt et al. 2012; McLellan et al. 2011; Pacheco-Torgal et al. 2014). Practical application of geopolymers in well cementing has been proposed as early as 2008 by a cementing services company (Barlet-Gouedard et al. 2008), with reports of field tests dating from the same period (Mahmoudkhani et al. 2008). Despite fulfilling rheological and pumpability requirements, having excellent mechanical properties at the hardened state and high durability in wellbore conditions (Chamssine et al. 2022a; Khalifeh et al. 2014; Nasvi et al. 2014a, 2014b, 2014c, 2014d; Paiva et al. 2018; Salehi et al. 2017, 2018, 2019), compared to OPC well-cementing pastes, geopolymers are not in widespread use in the oilwell industry. Salehi et al. (2018) attribute this fact to uncontrolled thickening time at elevated temperatures.

In the field of geopolymer technology, geopolymers are classified as two-part system (conventional geopolymers) or one-part system (JAW). Conventional geopolymers are formed by mixing one or more of the raw materials (precursors) with a high alkaline activator solution, producing a cementitious material. Activator solutions are generally composed of alkali metal hydroxide solutions, alone or combined with alkali metal silicates (Davidovits 1991, 2013). Common precursors are natural minerals, such as kaolin, metakaolin, aplite, and granite; industrial wastes, such as ground granulated blast furnace slag (GGBFS); fuel ashes, including fly ash, rice husk, bamboo leaf, and palm oil ashes; demolition wastes; and, more recently, red mud waste (Krishna et al. 2021). Geopolymers derived from rock-based precursors, such as aplite (Khalifeh et al. 2016a, 2016b, 2017, 2018, 2019) and granite (Alvi et al. 2020; Chamssine et al. 2021, 2022a, 2022b; Kamali et al. 2020, 2022), combined with GGBFS, have also been investigated for oil and gas applications, aiming to minimize their CO_2 emissions, compared to calcined precursors such as metakaolin and fly ash.

Logistics, health, safety, and environmental aspects related to the transportation and handling of alkaline activator solutions needed for mixing the two-part geopolymers in offshore applications are drawbacks for their field applications. In addition, the transportation of large volumes of the liquid hardener phase can produce additional CO_2 emissions when compared to a single-phase geopolymer powder system. These challenges highlight the importance of developing the one-part geopolymers, as a crucial strategy for their offshore oilwell-cementing applications, promoting its commercialization. Researchers have come up with the one-part system, known as the JAW system. In the JAW system, the alkaline/alkali silicate solution is replaced with a powder phase and preblended with the precursors. So, only water

*Corresponding author; email: mohamed.a.omran@uis.no

Original SPE manuscript received for review 21 December 2022. Revised manuscript received for review 26 April 2023. Paper (SPE 215825) peer approved 18 May 2023.

is required to be introduced to the powder to produce the slurry. Such a product would then potentially be capable of being user-friendly at the same time as generating lower CO_2 emissions, rooted in the transportation of unnecessary liquid (Omran and Khalifeh 2023; Wan-En et al. 2022).

Pacheco-Torgal et al. (2008) and Singh and Middendorf (2020) discussed views on the geopolymerization reaction, summarizing the process as a dissolution of the precursors in the alkaline solution as the pH is raised, followed by the transport and reorganization of simple silica and alumina tetrahedra, condensation in dimers and oligomers, and polymerization of the aluminosilicate network **(Fig. 1).**

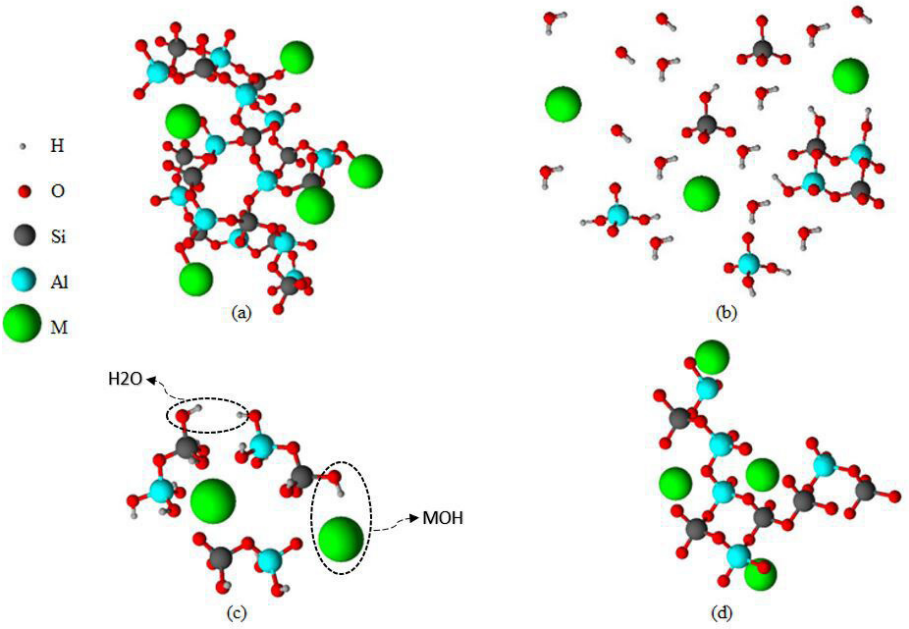

Fig. 1—Geopolymerization process steps: (a) geopolymer precursor prior dissolution, (b) dissolution and formation of monomers and dimers, (c) reorganization and condensation, and (d) geopolymerization.

The product of the geopolymerization process is a solid 3D network of silicate and aluminate tetrahedra, incorporating positively charged cations (mainly Na^+, K^+, and Ca^{2+}) to balance the charge of aluminate. Usually, the resulting network is denoted N-A-S-H (sodium ions), K-A-S-H (potassium ions), or (C, N)-A-S-H (calcium and sodium), where (H) represents free water in the nanopore space (Davidovits 2017; Khale and Chaudhary 2007). This must be distinguished from the C-S-H derived structures C-A-S-H and C-(N)-A-S-H, which form when enough calcium is present in solution. These structures maintain the classic lamellar structure of C-S-H, with partial replacement of silicate by aluminate tetrahedra and incorporation of sodium into the interlamellar solution (Myers et al. 2014). These products are more usually associated with alkali-activated materials, rather than geopolymers. Hybrid AAM-geopolymer pastes may form, with (C,N)-A-S-H slowly changing into C-(N)-A-S-H as the paste matures (García-Lodeiro et al. 2013).

The kinetics of geopolymer formation is still not completely understood, and there is no single technique that quantifies the reaction progress across all steps (Luukkonen et al. 2018; Zhang et al. 2012, 2013). Most often, the authors study the overall kinetics through practical measurements, such as the setting time and strength development rate, regardless of precursors, activators, and retarders used. Zhang et al. (2012) described the heat release rate of metakaolin-based geopolymer during isothermal calorimetry, identifying three distinct peaks. Peak I is a sharp peak that occurs after mixing, interpreted as the heat of dissolution of the precursors, followed by an intermediate period of lower heat release rate, during which reorganization and condensation occur. Peak II corresponds to geopolymerization and percolation of the solid phase. A third peak was observed, but its meaning is still unclear. This two-step heat release behavior was observed by other researchers too (Cai et al. 2020; Kumar et al. 2010; Paiva et al. 2021; Yao et al. 2009), sometimes with significant overlap between the two peaks. In contrast with OPC hydration, there is no direct proportion between heat release and reaction progress. The amount of heat reflects the enthalpy of formation of the specific products formed. In particular, K-A-S-H formation releases more heat than the equivalent amount of N-A-S-H (Paiva et al. 2021).

Nedunuri and Muhammad (2022) reviewed retarders for alkali-activated materials and reported that only zinc was able to delay setting by forming complexes with both silica and calcium ions. The authors studied the effect of up to 3% $ZnSO_4 \cdot 7H_2O$ on the properties of alkali-activated GGBFS and fly ash at room temperature, finding it very effective in increasing both initial and final setting times. However, increasing the concentration of zinc delayed strength development in the first 7 days, leading to a lower final strength. In extreme cases, formulations with 11% or less CaO in the precursor mix and 3% zinc did not develop any strength after 120 days, suggesting a poisoning effect. Zailan et al. (2020) were able to add up to 10% ZnO to a Type F fly ash-based geopolymer, with a decrease of 44% in the compressive strength at 28 days, but the authors did not report the effect in setting time. Wang et al. (2020) observed a significant increase in setting times after adding 25% ZnO by weight of metakaolin. The authors attribute the effect to the formation of sodium or potassium zincate, retarding the formation of geopolymer. However, the amount of zinc is much larger than typically used for retardation purposes, and the compressive strength was not reported.

The zinc retardation mechanism was studied by Garg and White (2017) in alkali-activated slag using ZnO, concluding that calcium zincate $Ca[Zn(OH)_3]_2 \cdot 2H_2O$ (CZ) precipitates as a metastable phase, delaying the formation of C-(N)-A-S-H. The authors did not observe any retardation of alkali-activated metakaolin, suggesting that retardation is dependent on the presence of calcium. After the ZnO is consumed, the calcium concentration rises, and C-(N)-A-S-H starts to form. At this point, CZ starts to dissolve, calcium is released, and zinc is incorporated into the C-(N)-A-S-H network, replacing silica tetrahedra (Tommaseo and Kersten 2002).

Considering there is no literature consensus on the zinc retardation mechanism and its optimal concentration for low-calcium geopolymer systems, Chamssine et al. (2021) studied a two-part low-calcium (10%) geopolymer well-cementing system. Their precursors were granite, GGBFS, and silica, and they found that the addition of $Zn(NO_3)_2{\cdot}6H_2O$ and $K(NO_3)$ was able to extend the setting time. Chamssine et al. (2022b) reported that the addition of 0.3% Zn^{2+} by weight of slurry as zinc salt extended significantly the thickening time at 50°C of bottomhole circulating temperature (BHCT) and 14 MPa of curing pressure. Chamssine et al. (2022a) increased the Zn^{2+} addition to 1.1% by weight of slurry and prolonged the pumpability at 60°C BHCT and 14 MPa.

One-part geopolymers are a more recent development, combining suitable precursors and activators in a solid mixture that forms a geopolymer by the simple addition of water (Luukkonen et al. 2018). The precursors can be any materials that form conventional geopolymers, and the activators can be prepared using the components of any two-part geopolymer activator solutions. Additionally, no differences were found in the reaction products of one- and two-part fly-ash geopolymers when prepared with similar mixing ratios (Suwan and Fan 2017). However, an important difference between two- and one-part geopolymers is the slow release and availability of alkali and free $HSiO_4^{3-}$ and $Al(OH)_4^-$, which may hinder or prevent the geopolymerization reaction. Mitigation techniques include adding reactive sources of silica and alumina, such as amorphous silica and sodium silicates and aluminates, calcinating the precursors, grinding the precursors to increase their surface area, and grinding the precursors with the alkali sources to obtain mechanochemical activation (Matalkah et al. 2017). However, finely ground precursors not only increase the availability of reactive species but also lead to worse rheological properties due to increased surface area. This is an important issue because commonly used OPC superplasticizers have mixed results for one- and two-part geopolymers, depending on alkalinity, activator type, precursor type, calcium content, and temperature (Nematollahi and Sanjayan 2014; Omran et al. 2022a, 2022b; Palacios and Puertas 2005). Finally, when the precursors are sufficiently reactive, the added dissolution heat of activators may lead to the early setting of one-part geopolymer mixes.

The development of user-friendly geopolymers is a crucial strategy to facilitate the use of geopolymers as a full replacement of cement for oilwell cementing applications. Thus, the development of one-part geopolymers that require only the addition of water has become crucial in recent years. One-part JAW geopolymers are user and environmentally friendly cementing materials. They are more promising for in-situapplications due to overcoming the impracticalities of conventional two-part geopolymers (Omran and Khalifeh 2022, 2023).

Building on the previous works, Omran and Khalifeh (2022, 2023) proposed a novel one-part geopolymer formulation based on granite, GGBFS, and microsilica, using anhydrous potassium silicate as a solid activator. Four different solid admixtures were individually investigated, namely, NaOH, $CaCO_3$, CaO, and ZnO, in quantities ranging from 0.14% to 1.14% by weight of precursor. In addition to distilled water, a small amount of KOH solution was used as an accelerator. The neat formulation (W1Pb) developed 4.8 MPa in 7 days of curing at 70°C and atmospheric pressure. The use of calcium oxide, calcium carbonate, and NaOH resulted in a reduction of early strength, up to 7 days, even in the smallest concentration (0.14%), with worse effects in larger concentrations. NaOH had the worst performance, yielding 2.2 MPa at 7 days. Zinc oxide significantly improved the mechanical strength, reaching 9.5 MPa in 7 days by only using 0.14% ZnO. The authors concluded that the formulations with zinc oxide addition less than or equal to 0.86% have the potential to be used in oilwell cementing. While the addition of ZnO higher than 1.0 wt% showed a negative effect on the 24-hour compressive strength at 70°C.

Motivated by that, this paper aims to thoroughly evaluate the early age properties and the mix design of one-part rock-based geopolymer systems with 0.57% and 0.86% of ZnO, by investigating their geopolymerization process under an oilwell cementing condition. Consequentially, it is to design a new one-part naturally occurring viable and sustainable granite-based geopolymer. It is focused on studying each stage of the geopolymerization process starting from the characterization of dissolution, reorganization, and then polycondensation processes, integrating them with a wide range of physical and chemical characterizations.

Materials and Methods

Materials. The JAW geopolymer formulation is based on solid precursors and activator components, which are mixed with water to produce the cementing system. The precursor materials used were ground granite (from Norway), a rock-based aluminosilicate material; GGBFS (from Sweden), a calcium silicate material rich in aluminum and magnesium; and a small portion of microsilica (MS, from Norway), an almost pure amorphous silica.

This study is a design of granite-based geopolymers where the base of the JAW system is granite, and due to its chemical composition, it is normalized with microsilica and slag. Unlike GGBFS-based geopolymers, granite-based geopolymers are characterized as aluminosilicate-rich materials with low calcium content and less calcium dependency on geopolymerization reaction. In other words, GGBFS and microsilica were incorporated as composition normalizers to the total weight of the granite-based precursor, to develop the required early-age well-cementing properties (Omran et al. 2023).

Chemical Composition (wt%)	Granite	GGBFS	Microsilica	JAW Precursor Mixture
SiO_2	73.44	35.78	95.50	56.63
Al_2O_3	13.33	12.72	0.70	12.47
Fe_2O_3	2.06	0.18	0.30	1.09
MgO	0.44	12.77	0.50	6.23
CaO	1.12	33.74	0.40	16.45
Na_2O	3.12	0.55	0.40	1.77
K_2O	5.11	0.82	1.00	2.87
TiO_2	0.23	2.23	0.00	1.16
MnO	0.04	0.58	0.00	0.29
LOI*	0.90	0.30	2.00	0.60

* Loss on ignition.

Table 1—Chemical composition of the precursors.

The chemical composition, as well as the JAW precursor mixture composition, obtained through X-ray fluorescence analysis, is presented in **Table 1.** The physical properties of the precursors and other mixture components are presented in **Table 2.** Their specific gravities at 25°C were determined with an Ultrapyc 3000 Helium pycnometer from Anton Paar. The particle-size distributions of the solid precursors **(Fig. 2)** and their estimated specific surface areas were assessed through laser diffraction in water dispersion, using a Malvern Mastersizer 3000 particle size analyzer with size limitations over 3000 µm.

The activators were prepared using anhydrous potassium silicate with a molar ratio (SiO_2/K_2O) of 3.92 and ground potassium hydroxide pellets. When required by the specific formulation, KOH and distilled water were used to prepare a 12 M solution. Zinc oxide was

Physical Properties	SG (g/cm^3)	d_{10} (µm)	d_{50} (µm)	d_{90} (µm)	SSA (m^2/kg)
Granite	2.63	3.52	21.1	131	631
GGBFS	2.90	2.79	15.9	46.6	944
Microsilica	2.29	0.19	0.34	0.60	19 320
K_2SiO_3	2.37	ND	ND	ND	ND
KOH (anhydrous)	2.12	ND	ND	ND	ND
ZnO	5.61	ND	ND	ND	ND

ND, not determined; SG, specific gravity; SSA, specific surface area; d_{10}, d_{50}, d_{90}, particle-size distribution percentiles.

Table 2—Physical properties of the components.

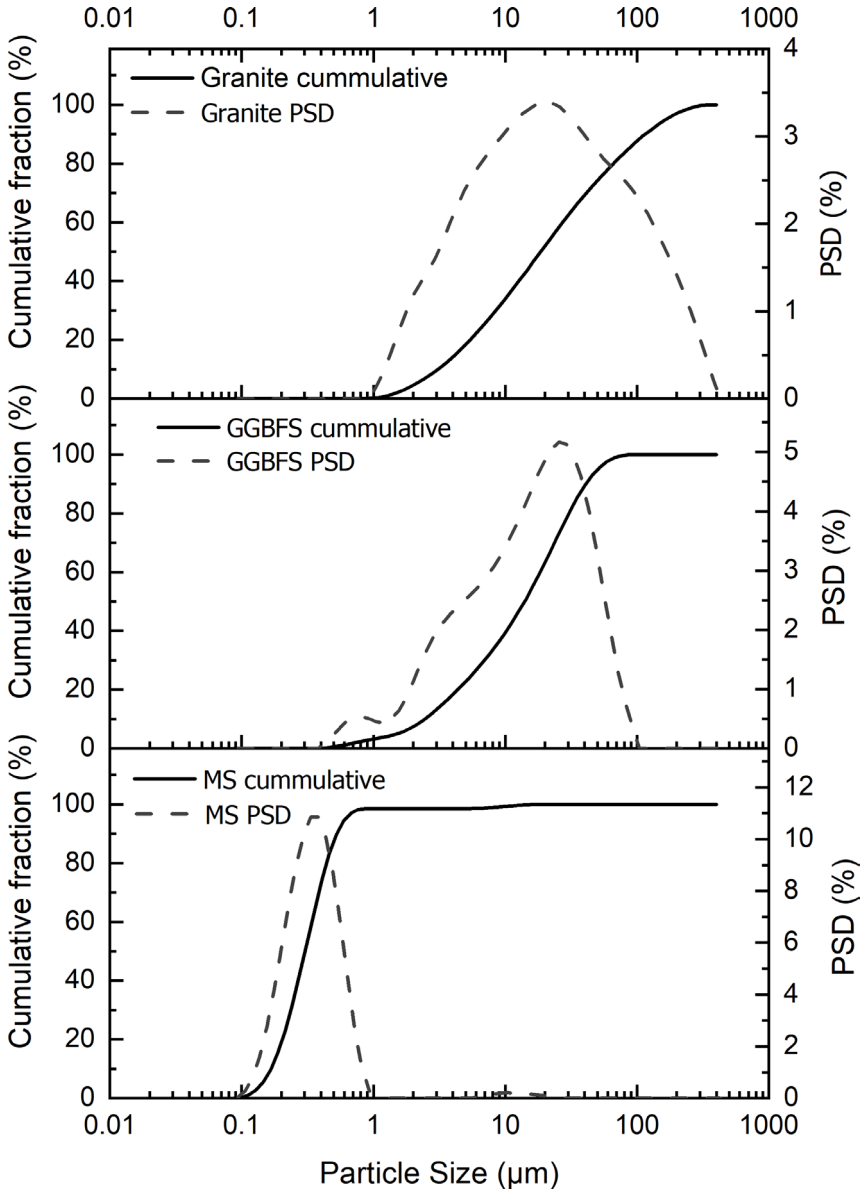

Fig. 2—Size distribution of precursors in aqueous dispersions.

used as an additive to improve the mechanical properties and potentially retard the setting at high temperatures. Distilled water was used to prepare the samples. When the KOH solution was used, its water content was discounted from the added water.

Formulations. In this work, three previously developed formulations (W1Pb, W1Pb-Z4, and W1Pb-Z6) are studied using the following notation (neat, 0.57% ZnO, and 0.86% ZnO). Additionally, a true JAW neat formulation is introduced, in which the 12 M KOH solution is replaced by anhydrous potassium hydroxide and, therefore, only water is truly required in the liquid part. The silica modulus or molar ratio (SiO_2/K_2O) of the activator was kept constant at 2.40. The full compositions are listed in **Table 3,** while the molar ratios of those formulations, water-to-solid proportions, and their theoretical specific gravities are listed in **Table 4.**

Composition (% bwop*)	Granite	GGBFS	MS	K_2SiO_3	KOH (Anhydrous)	KOH (12 M Solution)	ZnO	Water
JAW	48.6	47.1	4.29	20.8	4.24	0.00	0.00	41.3
Neat	48.6	47.1	4.29	20.8	0.00	9.21	0.00	36.4
0.57% ZnO	48.6	47.1	4.29	20.8	0.00	9.21	0.57	36.4
0.86% ZnO	48.6	47.1	4.29	20.8	0.00	9.21	0.86	36.4

*By weight of precursor mixture (granite, GGBFS, and MS).

Table 3—Geopolymer formulations investigated in this study.

Molar Ratios	JAW	Neat	0.57% ZnO	0.86% ZnO
$SiO_{2,nominal}/Al_2O_3$	9.72	9.72	9.72	9.72
$SiO_{2,reactive}/Al_2O_3$	4.87	4.87	4.87	4.87
$SiO_{2,nominal}/CaO$	4.05	4.05	4.05	4.05
$SiO_{2,reactive}/CaO$	2.03	2.03	2.03	2.03
K_2O/Al_2O_3	1.07	1.07	1.07	1.07
Na_2O/Al_2O_3	0.23	0.23	0.23	0.23
$(K_2O + Na_2O)/Al_2O_3$	1.31	1.31	1.31	1.31
$ZnO/SiO_{2,nominal}$	–	–	0.00585	0.00877
$ZnO/SiO_{2,reactive}$	–	–	0.0117	0.0175
ZnO/CaO	–	–	0.0237	0.0355
H_2O/K_2O	17.75	17.78	17.78	17.78
KOH molarity (M)	–	12	12	12
Water/solids	0.338	0.338	0.336	0.335
Specific gravity (g/cm^3)	1.88	1.90	1.90	1.89

Table 4—Oxide molar ratios, water-to-solid ratios, and theoretical density of geopolymer formulations.

Activation (pH) and dissolution [inductively coupled plasma mass spectrometry (ICP-MS)] studies were performed for a diluted version of the activator, for each individual precursor, for zinc oxide, and for the full formulations of **Table 3**. All solids were mixed with the diluted activator, as described in **Table 5.** For ICP-MS tests, the activator was diluted with double the amount of water.

The overall kinetics evaluation [differential scanning calorimetry (DSC)] used the same formulations of **Table 3** and additionally two individual precursor formulations presented in **Table 6.**

Mixing and Conditioning. Slurry preparation was performed by preblending all solid components with the activator (solid and/or solution) and adding the mixture to distilled water, in the amount indicated for each experiment. For pH, ICP-MS, and DSC tests, the solids were homogenized by mixing and shaking manually, then added to the activator in water, and hand mixed for 5 minutes.

For standard tests [e.g., thickening time, sonic strength (SS), and destructive compressive strength], the procedure recommended in API RP 10B-2 (2019) was followed. The OFITE Model 20 constant-speed blender was used for mixing all the slurry components. The preblend of geopolymer precursor and activator was poured in distilled water into the first 15 seconds at 4,000 rev/min, and then the slurry was sheared for 35 seconds at 12,000 rev/min.

A temperature of 50°C was chosen as BHCT and 70°C as the bottomhole static temperature (BHST). An atmospheric consistometer (API RP 10B-2 2019) was used for conditioning all slurries, at 50°C BHCT, prepared for measuring compressive strength.

X-Ray Diffraction. The mineralogical characterization of raw precursors **(Table 1)** and pastes **(Table 3)** was obtained by X-ray diffraction (XRD) and Rietveld analysis. Fractured paste samples from the uniaxial compressive strength (UCS) test were ground and dried in an oven at 30°C overnight, and then they were kept in a vacuum dryer for 1 day to maximize the removal of moisture. The analysis was conducted according to ASTM C1365-18 (2018) using a Bruker-AXS Microdiffractometer D8 Advance diffractometer, operating at 45 kV and 40 mA with CuKα radiation (λ = 1.5418 Å), a scanning range of 5–92° 2θ, and a step size of 0.01° 2θ.

Mix (% bwop*)	Granite	GGBFS	MS	K_2SiO_3	KOH (Anhydrous)	KOH (12 M Solution)	ZnO	Water†
K_2SiO_3	0.0	0.0	0.00	20.8	0.00	0.00	0.00	166
Activator	0.0	0.0	0.00	20.8	0.00	9.21	0.00	166
Granite	48.6	0.0	0.00	20.8	0.00	9.21	0.00	166
GGBFS	0.0	47.1	0.00	20.8	0.00	9.21	0.00	166
Microsilica	0.0	0.0	4.29	20.8	0.00	9.21	0.00	166
0.86% ZnO‡	0.0	0.0	0.00	20.8	0.00	9.21	0.86	166
JAW	48.6	47.1	4.29	20.8	4.26	0.00	0.00	166
Neat	48.6	47.1	4.29	20.8	0.00	9.21	0.00	166
0.57% ZnO	48.6	47.1	4.29	20.8	0.00	9.21	0.57	166
0.86% ZnO	48.6	47.1	4.29	20.8	0.00	9.21	0.86	166

*By weight of precursor used in the JAW mixture.
†For dissolution (ICP-MS) measurements, the amount of water was doubled to 333% bwop.
‡This composition was only considered for pH measurements.

Table 5—Precursor and geopolymer formulations adopted for the pH and ICP-MS evaluations.

Mix (% bwop*)	Granite	GGBFS	MS	K_2SiO_3	KOH (Anhydrous)	KOH (12 M Solution)	ZnO	Water
Granite	100	0.0	0.00	20.8	0.00	9.21	0.00	36.4
GGBFS	0.0	100	0.00	20.8	0.00	9.21	0.00	36.4

*By weight of precursor used in the JAW mixture.

Table 6—Precursor formulations adopted for the kinetics evaluations.

Crystalline phases of precursors and pastes were identified using the EVA v5 Bruker software. Rietveld quantitative phase analysis of granite was conducted using the TOPAS v5 Bruker software and a PDF database. GGBFS and MS are approximately amorphous, based on the absence of major crystalline peaks in their respective diffractograms.

Fourier-Transform Infrared Spectroscopy. Aliquots from the samples prepared for XRD tests (raw precursors in **Table 1** and geopolymer pastes in **Table 3**) were used for Fourier transform infrared (FTIR) spectroscopy according to the ASTM C1365-18 (2018) standard, using an Agilent Cary 630 FTIR spectrometer equipped with a diamond composite attenuated total reflectance crystal. FTIR spectra were collected in transmittance mode from 4000 cm^{-1} to 600 cm^{-1} at a resolution of 1 cm^{-1}.

Alkalinity and Inductively Coupled Plasma. A Mettler Toledo SevenExcellence pH meter was used to measure the alkalinity of diluted mixes **(Table 5)** at room temperature (uncontrolled) and BHCT (50°C). ICP-MS was used to analyze the dissolution of each material and their mixes **(Table 5)** in the given alkaline medium following ASTM D5673-16 (2016). The ICP-MS samples were collected after performing a 30-minute static fluid loss test (API RP 10B-2 2019) at room temperature and 6.9 MPa for each of the formulations given in **Table 5**.

Isothermal Calorimetry. A DSC was used to obtain the isothermal calorimetry curves of the raw materials and geopolymer pastes (**Tables 3 and 6**, respectively) to study their kinetics. Studies were performed at room temperature (25°C) and at BHCT (50°C) for up to 180 minutes. The heat evolution exerted by them was evaluated according to ASTM C1702-17 (2017).

Thickening Time. The thickening time of all geopolymer formulations, presented in **Table 3**, was measured according to API RP 10B-2 (2019) using an atmospheric consistometer, ramping up from room temperature to 50°C BHCT at 1 °C/min. The pumpability time at 40 Bc was chosen for all pastes, and the tests were ended by that time.

Ultrasonic Compressive Strength. The SS development of the pastes **(Table 3)** was assessed according to API RP 10B-2 (2019), with an ultrasonic cement analyzer. The test was performed at 13.8 MPa and 70°C (BHST) for 7 days, with the temperature and pressure ramp-up rates of 1 °C/min, and 17.2 bar/min, respectively. SS was obtained from the transit time using the custom algorithm fitted by Omran and Khalifeh (2022), which correlates the destructive uniaxial strength with the ultrasonic cement analyzer transit time, for a very similar formulation.

Uniaxial Compressive Strength. Cylindrical samples for UCS (51 mm diameter and 80 mm height) were cast in plastic molds and cured at atmospheric pressure in an oven at 70°C (BHST) for 24 hours and 7 days. A cutter machine was used to flatten both ends of the cured samples. Six samples for each mix design of **Table 3** were prepared. UCS tests were performed according to ASTM C597-16 (2021), using a Toni Technik-H mechanical tester at a loading rate of 10 kN/min.

Results and Discussion

Characterization of Precursors and Pastes (Particle-Size Distribution and XRD). As seen in **Table 1**, the chemical composition of the granite precursor is mainly silica and alumina, with potassium, sodium, and iron oxide as minor components. Its particle-size distribution (**Table 2** and **Fig. 2**) is very coarse and wide, spanning from 3.5 μm to 131 μm, with a median diameter of 21 μm. GGBFS, on the other hand, is composed mainly of silica and calcium oxide, with similar amounts of aluminum and magnesium as secondary components. Its median particle size of 16 μm is similar to that of granite, with a narrower range. Microsilica is almost pure silicon oxide, much finer than the other two precursors, and with a narrow size distribution of around 0.34 μm.

XRD spectra of the precursors, characterized by Omran and Khalifeh (2022), are shown in **Fig. 3.** Granite has a very high crystalline content, whose mineralogy was reinterpreted and quantified, as detailed in **Table 7.** The major phases are quartz, feldspar (microcline and albite), and oligoclase, with biotite and chlorite as minor phases.

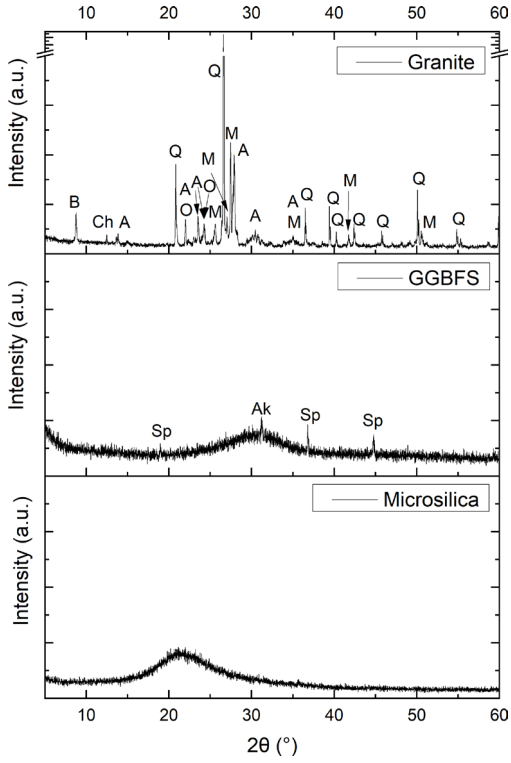

Fig. 3—XRD mineralogical characterization of the raw material precursors. (A) Albite, (Ak) Akermanite, (B) Biotite, (Ch) Chlorite, (M) Microcline, (O) Oligoclase, (Q) Quartz, and (Sp) Spinel.

Minerals	No.	Granite (%wt/wt)
Quartz	PDF 00-008-7651	35.693
Albite	PDF 00-009-0466	21.625
Microcline 1	CIF 9004191	16.059
Microcline 2	PDF 00-019-0932	11.918
Oligoclase	CIF 9011423	10.654
Biotite	PDF 04-013-2135	2.382
Chlorite	COD 9010163	1.669

Table 7—Granite mineralogy obtained from Rietveld quantification.

As GGBFS and microsilica exhibit mainly amorphous profiles, compared to granite, no Rietveld refinement was conducted for them. Qualitatively, GGBFS contains a minor amount of akermanite and spinel, as expected for typical blast furnace slags (Hewlett 2001).

XRD spectra of selected geopolymer pastes are shown in **Fig. 4.** In comparison with the solid precursors, the main peaks relative to granite (quartz, albite, and microcline) are still present, while the biotite peak disappeared. An additional hydrated K-A-S-H phase was observed in the pastes, JAW and neat. In 0.86% ZnO paste, an additional K-(K-Na)-Zn-A-S-H phase, with the presence of zinc, was detected. An amorphous hump is present in all pastes, which encompasses unreacted amorphous precursor phases, and possibly amorphous geopolymers and hydrated phases such as C-S-H, C-A-S-H, and C-(K, Na)-A-S-H.

FTIR Characterization of Precursors and Pastes. FTIR spectra were used to analyze the individual precursors and the dry potassium silicate activator at room temperature following ASTM E168-16 (2016). The broadband between 800 cm^{-1} and 1250 cm^{-1} is attributed

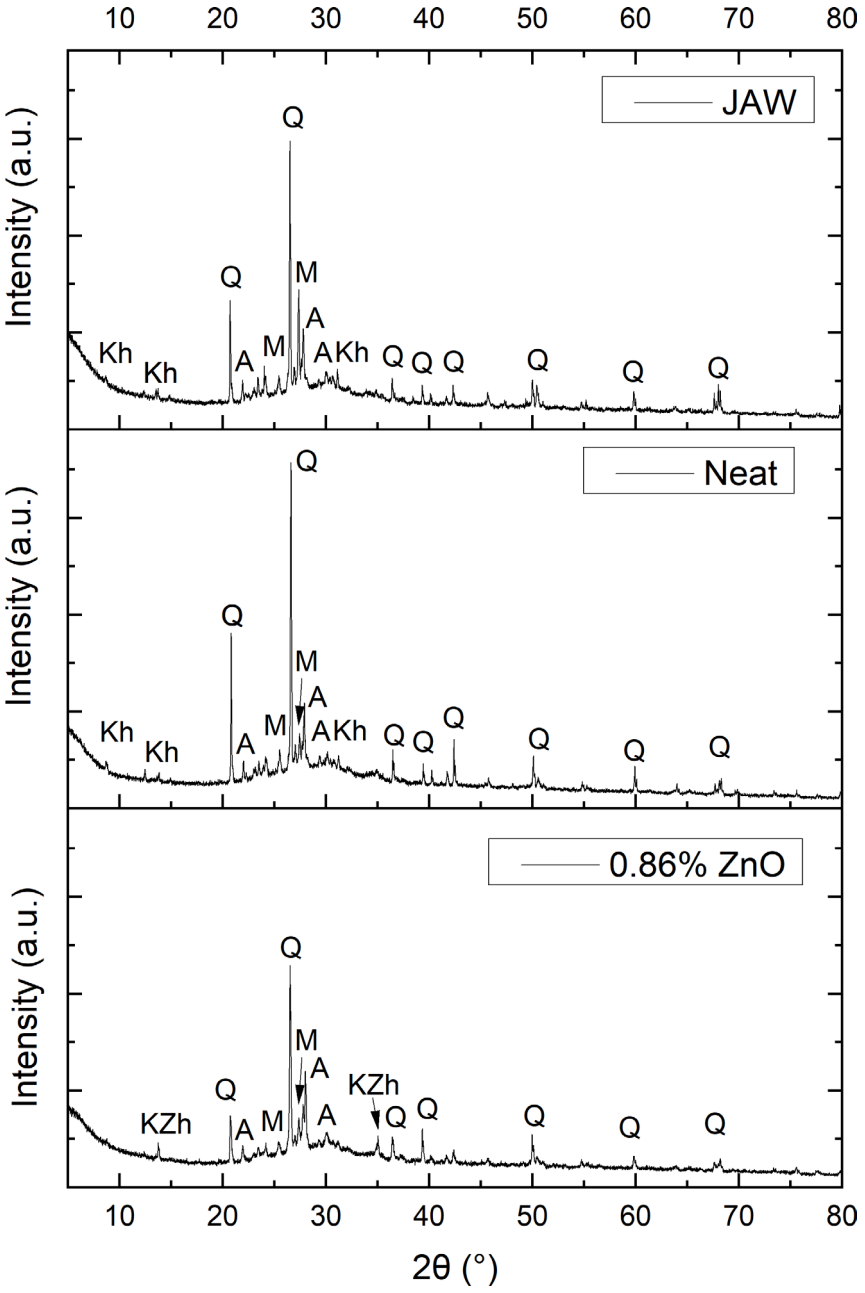

Fig. 4—XRD mineralogical characterization of selected geopolymers after 7 days of curing at 70°C. (A) Albite, (Kh) K-A-S-H, (KZh) (K-Na)-Zn-A-S-H, (M) Microcline and (Q) Quartz.

to the asymmetric stretching vibrations of the bond between silica tetrahedra or silica-alumina tetrahedra (Si-O-T, where T is either Si or Al) by Sturm et al. (2016). This band was observed for all materials, as shown in **Fig. 5,** with peaks varying from 990 cm^{-1} for granite to 872 cm^{-1} for GGBFS. Sturm et al. (2016) observed a peak at 1059 cm^{-1} for pure amorphous silica and a peak at 975 cm^{-1} for geopolymer, attributing the shift to the increasing fraction of alumina tetrahedra.

In the case of the silicate activators, Falcone et al. (2010) observed a shift from 1020 cm^{-1} toward lower wavenumbers with the increase in silica concentration. Therefore, the main absorption peak at 965 cm^{-1} is consistent with the high molar ratio (3.92) of the solid activator.

GGBFS also shows a small absorption peak at 1480 cm^{-1}, generally attributed to O–C-O bonds, such as those in calcium carbonate (Sturm et al. 2016). As GGBFS can form C-S-H, mild carbonation may have occurred in this precursor (Hewlett 2001).

FTIR spectra of the geopolymer pastes are presented in **Fig. 6.** The band between 800 cm^{-1} and 1250 cm^{-1}, corresponding to the stretching vibration mode of tetrahedral silica and alumina, was also observed. The peak at 965 cm^{-1} is located between the granite and GGBFS peaks and is consistent with the structure of geopolymers. The carbonate peak from GGBFS is still present around 1420 cm^{-1}, but less pronounced, suggesting that the geopolymer products are not suffering carbonation.

The broad hump between 2500 cm^{-1} and 3700 cm^{-1} corresponds to stretching vibrations of incorporated water and hydrated products (H–OH bonds). Together with the small O–H stretching peak around 1640 cm^{-1}, this peak around 3360 cm^{-1} represents the generation of geopolymeric products. Compared to JAW (dry activator), the peak area increases by 25% for the neat paste, due to the use of a liquid activator. The addition of zinc oxide does not shift any of the peaks but increases the area of the H–OH peak by 59% and 61% for 0.57% ZnO and 0.86% ZnO pastes, respectively, compared to the JAW one. The peak intensity follows the same trend.

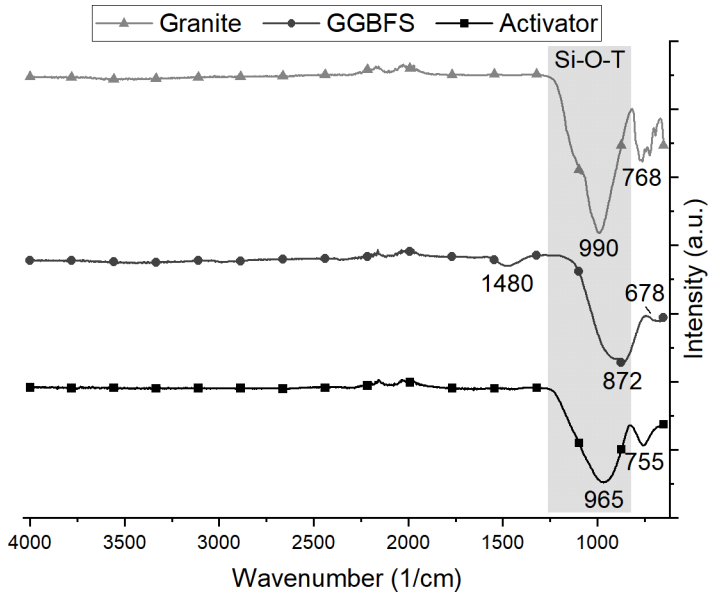

Fig. 5—FTIR spectra of the solid powder precursors.

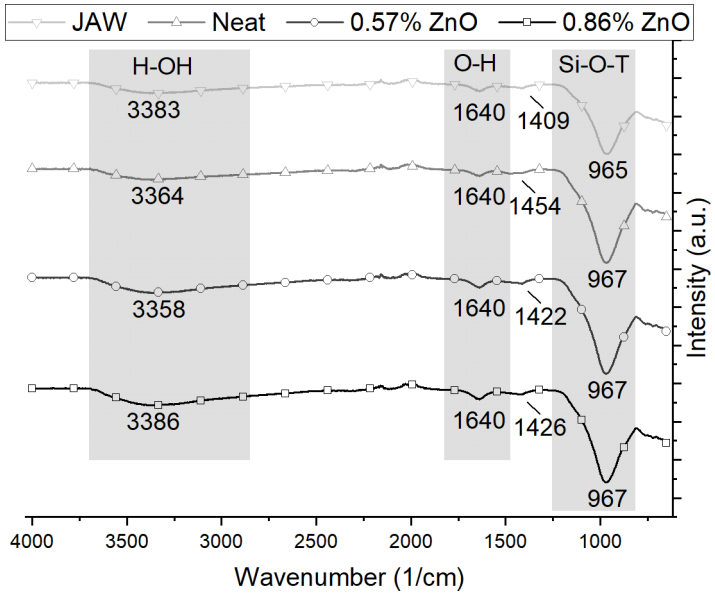

Fig. 6—FTIR spectra of the four geopolymer designs.

Activation of Precursors and Pastes (pH Evaluation). Table 8 presents the pH evolution in the first 10 minutes after mixing at room temperature. Pure silicate dissolves and generates a stable pH of 12.13. Therefore, in this dilute concentration, it is not sufficiently alkaline to be a standalone activator. The addition of KOH raised the pH to 13.48. Subsequent tests are analyzed with respect to this.

Granite initially increased the pH by +0.07 but then lowered by −0.02 after 10 minutes, showing some consumption of OH^- in the first minutes. GGBFS also reduced the pH by −0.05, a similar behavior. Microsilica had a stronger effect, lowering by −0.11, despite having less than 10% of the mass of the two other precursors. Zinc oxide also consumed alkalinity, lowering the pH by −0.05 despite its much smaller amount. This can be explained by its solubility in high pH. In this temperature and time scale, granite is less reactive than GGBFS, while microsilica seems to be more easily activated than the other two.

When combined, the precursors have a different effect on pH. Formulation JAW caused an initial decrease in pH but a final increase (+0.03), which can be explained by its use of solid KOH instead of the KOH solution used for the other tests. The dissolution of KOH can also explain the increase in solution temperature to 25.8°C. Formulation neat had an insignificant variation of pH. Mixes of 0.57% ZnO and 0.86% ZnO displayed an initial drop in pH, but 0.57% ZnO returned to the base value of 13.48. Only 0.86% ZnO lowered the pH by −0.08 after 10 minutes. As microsilica alone can lower the pH to 13.37 and each individual precursor can lower the pH below the base value, a competition effect must be inhibiting the activation of the mixes.

Table 9 presents the results at a temperature of 50°C. The results for precursors are analogous to those at room temperature. The baseline (pure activator) is pH 13.41 at 10 minutes. Granite had the smallest reduction (−0.03), GGBFS was again more reactive than granite (reduction −0.05) and microsilica had the largest effect (−0.11). Zinc oxide reduced the pH by −0.09, despite its very small amount. The formulations without zinc had an initial drop and stayed stable for 10 minutes at 13.30 (−0.11). The two formulations with zinc had a

Activators, Activated Materials, and Formulations	pH* (Initial)	pH* (10 Minutes)	T (°C) Average
K_2SiO_3	12.13	12.12	22.14
K_2SiO_3 + KOH (Activator)	13.50	13.48	22.53
Granite	13.55	13.46	22.43
GGBFS	13.50	13.43	22.47
Microsilica	13.47	13.37	22.55
0.86% ZnO†	13.47	13.43	23.00
Neat†	13.49	13.48	22.77
0.57% ZnO‡	13.45	13.48	22.87
0.86% ZnO‡	13.42	13.40	22.90
JAW‡	13.43	13.53	25.80

*pH meter has ±0.01 error margin.
†Same composition described in **Table 5**.
‡By weight of precursor used on each paste.

Table 8—Initial and final pH data at room temperature.

Activator, Activated Materials, and Formulations	Initial pH*	pH* After 10 minutes	pH Total Average
K_2SiO_3 + KOH (activator)	13.40	13.41	13.41
Granite	13.39	13.38	13.39
GGBFS	13.35	13.36	13.36
Microsilica	13.32	13.30	13.31
0.86% ZnO†	13.31	13.31	13.31
Neat‡	13.30	13.30	13.30
0.57% ZnO‡	13.27	13.26	13.27
0.86% ZnO ‡	13.27	13.25	13.26
JAW ‡	13.31	13.30	13.30

*pH meter has ±0.01 error margin.
†Same composition described iin **Table 5**.
‡By weight of precursor used on each paste.

Table 9—Initial and final pH data at 50°C.

slightly larger initial drop, ending with 13.26 (−0.15). This confirms that zinc oxide contributes to the reduction in pH, as suggested by the data at room temperature.

Dissolution of Precursors and Pastes (ICP Analysis). ICP-MS results for the activator, individual precursors with activator, and diluted geopolymer mixes are shown in **Table 10.** We use the pure activator (silicate and hydroxide solution) as the baseline for silicon (750 mg/L) and potassium (20 000 mg/L) concentrations because all mixes have the same amount of activator and dilution water. Granite increased the silicon concentration from 750 mg/L to 1200 mg/L, while GGBFS decreased it to 220 mg/L. A possible reason is the adsorption of silicate on the surface of GGBFS particles (Hewlett 2001) or formation of C-S-H. Microsilica, as observed in the pH studies, was very effective in releasing silica into the solution. Potassium levels were not affected within the precision of the method. Although

Material	Silicon (mg/L)	Aluminum (mg/L)	Potassium (mg/L)	Sodium (mg/L)	Zinc (mg/L)
Activator	750	0.74	20 000	100	0.68
Granite	1200	6.5	20 000	110	5.2
GGBFS	220	23	19 000	110	1.2
Microsilica	2800	2.1	20 000	100	3
JAW*	840	110	89 000	800	21
Neat*	1100	94	71 000	540	0.61
0.57% ZnO*	900	120	64 000	540	980
0.86% ZnO*	530	140	60 000	530	1900

*By weight of precursor used on each paste.

Table 10—ICP evaluation for precursors and geopolymer pastes.

alumina contents in GGBFS and granite are similar (12.7% and 13.3%, respectively), GGBFS released much more aluminum (23 mg/L) than granite (6.5 mg/L).

Dilute geopolymer formulations show dissolution behaviors beyond the dissolution of each individual precursor. Notably, the silicon concentration of the mixes is smaller than that generated by granite by itself and much smaller than that of microsilica. Therefore, a phenomenon such as GGBFS surface adsorption or C-S-H formation must be consuming the silicate as it is released. On the other hand, all mixes release much more aluminate into the solution, compared to the sum of the precursors. This may be explained by noting that the decrease in silicate concentration favors the dissolution of silico-aluminates. The high amount of aluminum released by GGBFS may have the same origin. Potassium concentration is much higher for geopolymer mixes than for individual precursors and pure activators. About 77% of the potassium content of the mix comes from the activator; therefore, the increase in concentration must come from improved solubilization of solid potassium silicate.

The main effects of zinc oxide are a decrease in silicate concentration, a small increase in aluminate concentration, and a decrease in potassium concentration. Zinc oxide in water forms zincate, which captures silicate in zincate-silicate complexes. The simultaneous decrease in silicate and potassium concentration suggests the capture or precipitation of potassium zincate silicate, which would also explain the reduction in pH observed in the previous section. XRD analysis of cured geopolymers indicates the presence of a potassium-sodium zinc silicate hydrate (N, K)-Z-S-H, which could account for this observation. Aluminum concentration is not reduced, suggesting that aluminate is not being immobilized. Without calcium concentration measurements, it is not possible to confirm the precipitation of CZ, as suggested by Garg and White (2017), which would also be consistent with the observations.

Kinetics of Precursors and Pastes. For all DSC curves, the initial equilibration period is discarded, and the curves are shown after they become exothermal. The main difference in behavior between the curves at 25°C and the corresponding 50°C curves is that the main peak occurs earlier and has greater intensity and decays faster at 50°C, showing that the reactions are thermally activated. In most cases, the total heat released at 50°C is also larger during the first 3 hours.

Fig. 7 shows the heat evolution and accumulated heat released by precursors, for the first 3 hours after mixing. Compared to granite at 25°C, GGBFS reaches its peak heat release earlier and releases more heat during the study period. This can be understood as GGBFS has a significant amorphous fraction, which is more readily dissolved, compared to the mainly crystalline granite. At longer times, GGBFS releases more heat per unit weight, suggesting that the precursor can react further in the next hours. At 50°C, temperature activation makes both precursors approximately equivalent in peak heat release rate, but GGBFS sustains the reaction for longer. In fact, granite heat release appears to reach a plateau and the total energy is lower at 50°C than it is at 25°C.

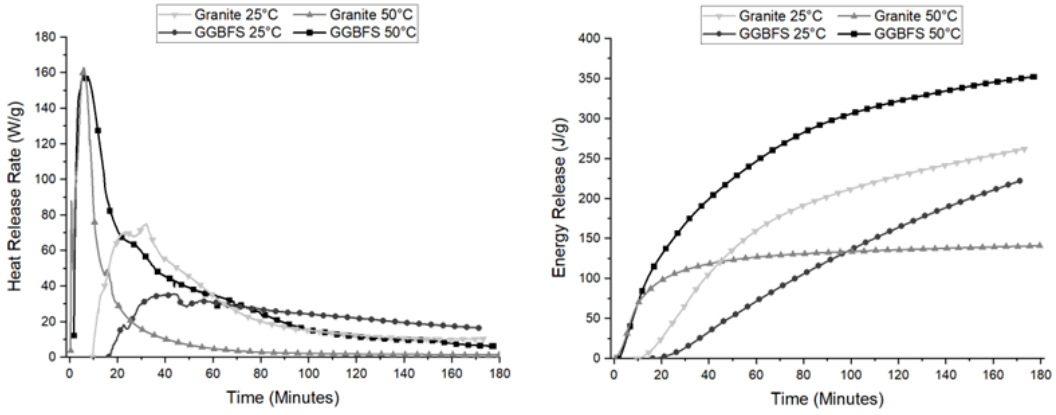

Fig. 7—DSC measurements of activated precursors at 25°C and 50°C.

As shown in **Fig. 8,** at 25°C, the neat paste with the liquid accelerator reacts earlier and has a larger heat release peak than the JAW paste with solid precursors. The total heat release is also higher for the neat slurry. This can be explained by the need to first dissolve the

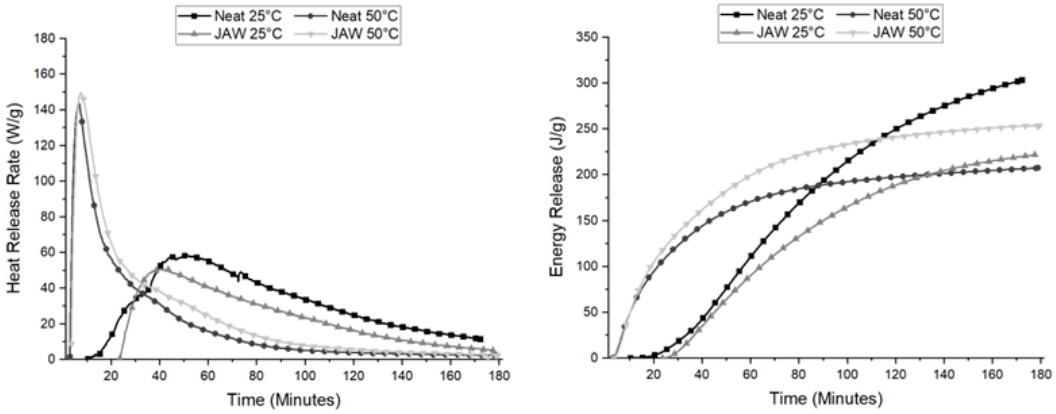

Fig. 8—DSC measurements of geopolymer formulations with liquid activator (neat) and solid activator (JAW) at 25°C and 50°C.

solid activator, before ideal conditions for precursor dissolution and geopolymerization can be met. At 50°C, this first dissolution step happens very fast, and the JAW was able to release more heat than the neat, possibly because of the significant heat of dissolution of potassium hydroxide.

Fig. 9 compares the heat evolution of the neat formulation vs. the ones with 0.57% ZnO and 0.86% ZnO. As the amount of added zinc increases, the height and width of the peak increase and the total amount of heat also increases. However, this early energy release is followed by a period of low heat evolution.

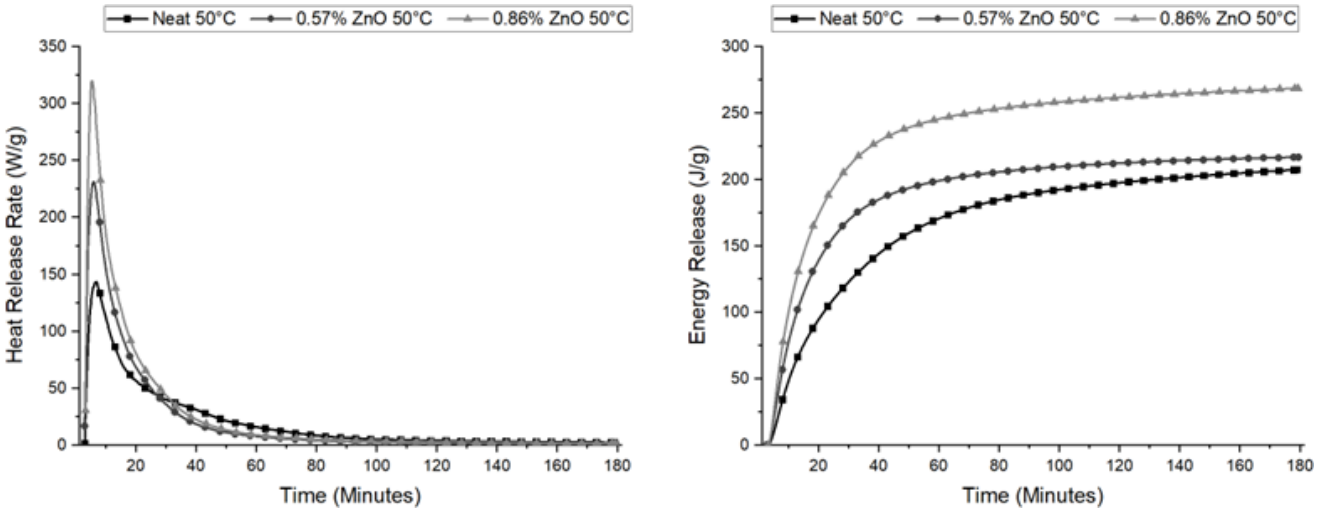

Fig. 9—Isothermal calorimetry measurements of geopolymer formulations with added zinc oxide at 50°C.

Table 11 summarizes the observations above in terms of the size and position of the peak in the heat evolution curve, as well as the total energy release for those pastes.

	Time at Maximum Heat Release Rate (minutes)		Maximum Heat Release Rate (mW/g)		Total Energy Release at 180 minutes (J/g)	
Material	25°C	50°C	25°C	50°C	25°C	50°C
Granite	44	6	35	152	216	140
GGBFS	24	6	65	162	257	347
JAW	39	8	50	140	217	251
Neat	52	8	57	143	298	205
0.57% ZnO	–	7	–	234	–	215
0.86% ZnO	–	7	–	317	–	267

Table 11—Heat and energy evolution parameters for the pastes.

Thickening Time. The consistency (in Bearden units) vs. time measurements at BHCT 50°C for the proposed geopolymer formulations are presented in **Fig. 10.** A consistency of 40 Bc was selected as a baseline for the pumpability period for geopolymer slurries. These consistency curves show the three geopolymerization reaction stages, starting from the dissolution of the precursors, observed as a decrease in consistency while the temperature is ramping up, until reaching the reorganization stage. The reorganization stage has the lowest consistency range. After that, the polycondensation stage starts, when the slurries coagulate and then transform into a gel with the formation of a 3D network polymeric structure. This rapid gain in consistency is usually called "right-angle set," and it is a desirable property in a well cementing slurry. Due to safety reasons, the tests were not followed up to 100 Bc.

These four rock-based slurries had pumpability times of 40 Bc ranging from 43 minutes to 45 minutes, as shown in **Fig. 10**. In addition, a right-angle set was observed for the four recipes. Compared to two-part rock-based slurries (Chamssine et al. 2021, 2022b), these recipes range from 64% to 72% of the pumpability time of those slurries. In contrast, the four mixes have initial consistencies from 17 Bc to 27 Bc, whereas the neat two-part slurry had initial consistency of around 37 Bc. Moreover, the JAW slurry had the lowest initial consistency among all one-part (neat, 0.57%, and 0.86% ZnO) rock-based geopolymer slurries due to the 100% free water content in liquid phase, while the rest have 88% free water content in liquid phase.

Ultrasonic Compressive Strength. Fig. 11 presents the SS development curves for the four geopolymer mixes at 70°C of BHST and pressurized to 2,000 psi (13.8 MPa). **Table 12** presents the conventional setting and hardening times, defined as the times to reach SSs of 100 psi and 500 psi (0.69 MPa and 3.45 MPa, respectively) in addition to the SS after 1 day and 7 days.

Uniaxial Compressive Strength. Fig. 12 shows the UCS of the geopolymer pastes after 1 day and 7 days of curing at 70°C and atmospheric pressure. JAW and neat slurries have similar strengths. Pastes with 0.57% and 0.86% ZnO have higher strength, almost

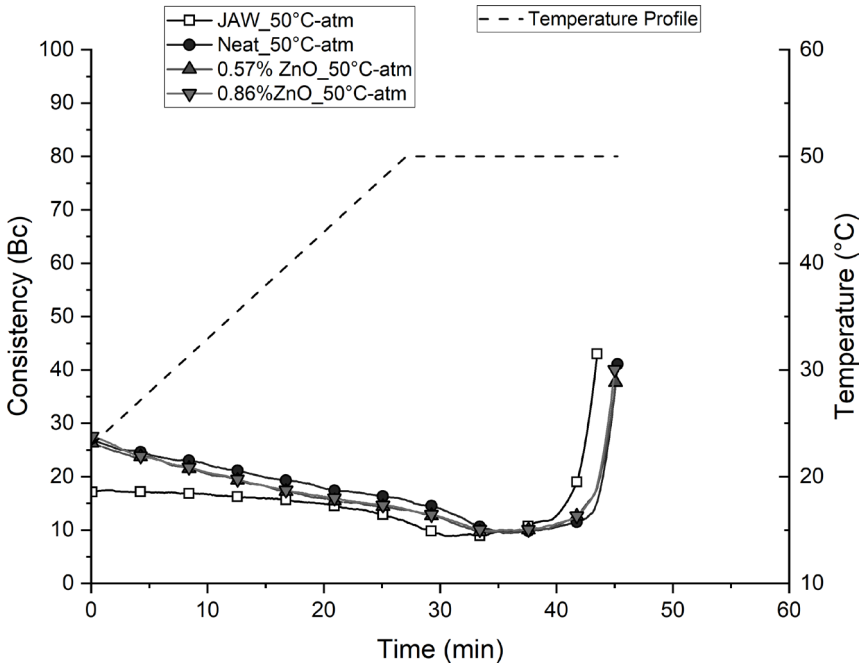

Fig. 10—Consistency evolution of geopolymer slurries at BHCT 50°C and atmospheric pressure.

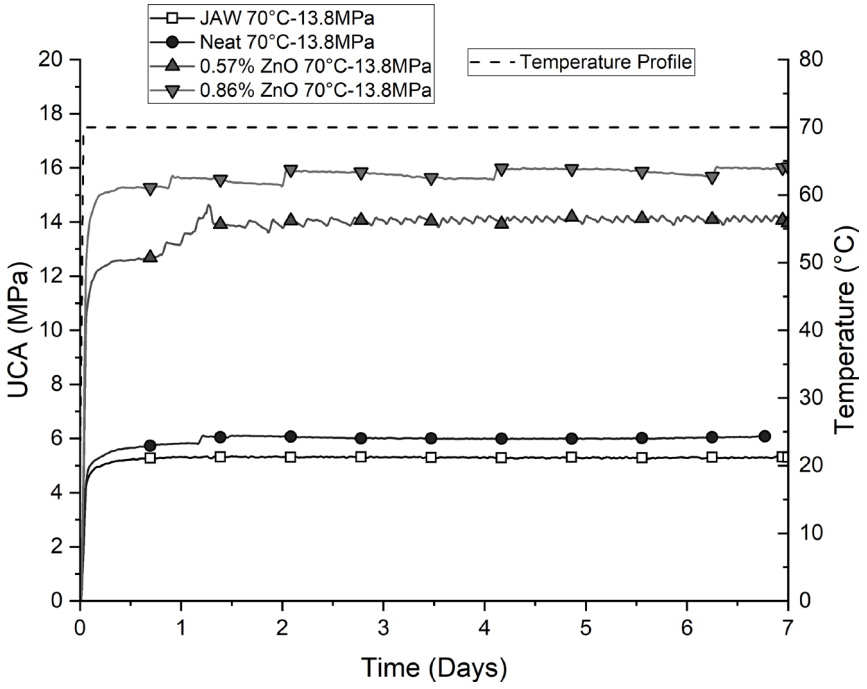

Fig. 11—SS development up to 7 days at 70°C and 13.8 MPa.

Mix Design	Setting Time to 100 psi (minutes)	Hardening Time to 500 psi (minutes)	SS (MPa) for 1 day	SS (MPa) for 7 days
JAW	44	68	5.36	5.42
Neat	43	66	5.85	6.10
0.57% ZnO	42	48	13.21	13.94
0.86% ZnO	38	46	15.65	16.04

Table 12—Summary of ultrasonic cement analyzer data for the four optimized mixes.

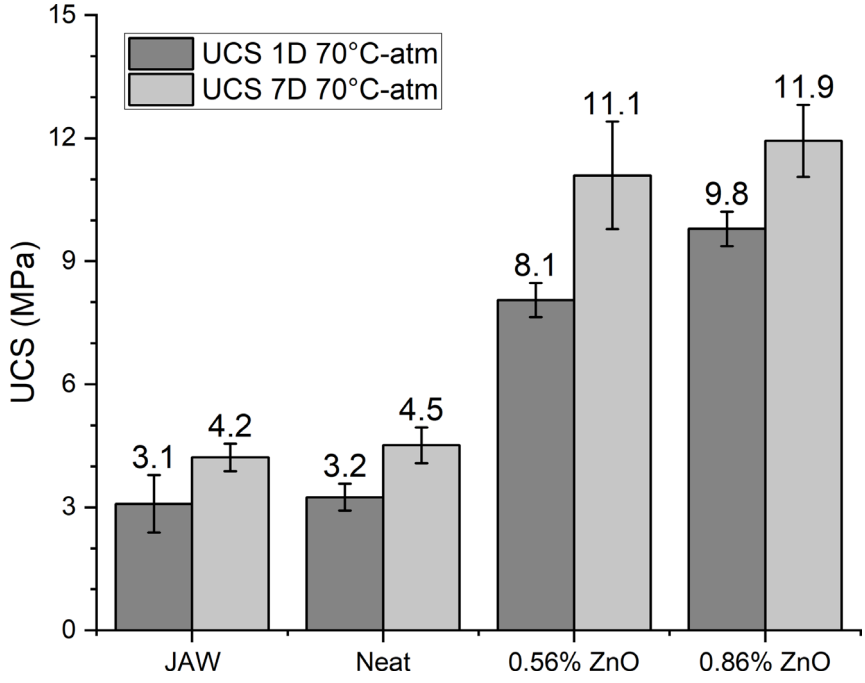

Fig. 12—UCS data cured at 70°C and atmospheric pressure.

three times the strength of the neat pastes. These results are in good agreement with those obtained using SS tests. Most of the strength development occurs within the first 12 hours.

Discussion

The JAW geopolymer formulation is a combination of two precursors with distinct natures and behaviors. Granite is a highly crystalline aluminosilicate material; therefore, it is slower to activate than amorphous precursors. Its silica/aluminum ratio is very high, compared to the ideal 2:1 ratio; therefore, geopolymerization in the form of K-A-S-H is limited by the low availability of aluminates in solution. On the other hand, GGBFS is a calcium-rich amorphous precursor, with less silica but similar aluminate content. It will dissolve earlier and supply free calcium to the solution. In low-pH silica-rich environments, this will lead to the formation of C-S-H (Myers et al. 2014), which will capture and precipitate silica, as observed through ICP **(Table 10)**.

Gasteiger et al. (1992) investigated the solubility of aluminosilicate materials in alkaline solutions, finding an equilibrium involving aluminate $Al(OH)_4^-$, orthosilicic acid $HSiO_4^{3-}$, and the solid phase present in the system, described by the solubility product [Si][Al]. In **Fig. 13,** the reduction in silica concentration will induce silicate-aluminate dissolution, especially after the addition of ZnO, favoring the silica/aluminum ratio close to the ideal ratio by increasing the availability of more free aluminum ions and enabling the formation of C-A-S-H, C-(K)-A-S-H, and (K-Na)-Zn-A-S-H.

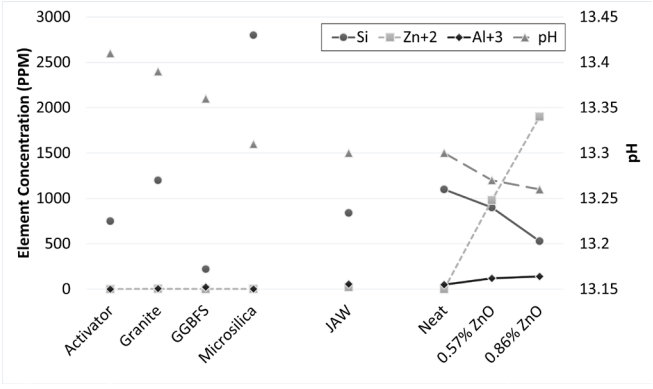

Fig. 13—Integrated analysis between pH and ICP for all given mixes.

When the precursors are combined in the JAW and neat formulations, it is observed through ICP-MS that higher silicate and aluminate concentrations can be obtained by the dissolution of silicate- and aluminate-rich granite, enhanced by the capture of silicates through C-S-H formation, using calcium from GGBFS, as seen in **Fig. 13**. Heat release peaks are broader than the respective peaks for each precursor, as the formulation starts to react earlier through the action of GGBFS and continues for longer as the granite fraction is consumed together with GGBFS.

At high pH, silica dimers and polymers tend to depolymerize. However, when sufficient aluminum and silica are present in solution, aluminosilicate dimers $[(OH)_3–Al–O–Si–(OH)_3]^-$ will form, reorganize, and condense in small aluminosilicate units (Gasteiger et al.

1992). In these conditions, zinc oxide is present as zincate, $Zn(OH)_3^-$, or $Zn(OH)_4^{2-}$ (Chen et al. 2012). Anseau et al. (2005) used ^{29}Si, ^{27}Al, and ^{67}Zn NMR in high pH solutions, to show that silicates in solution form complexes with both zincates and aluminates, in similar proportions. Each zincate ion can bind to a silicate monomer or dimer, while aluminates bind to a single silicate monomer. This competition may explain the retardation of low calcium geopolymers, as observed by Chamssine et al. (2022b).

In the case of 0.57% ZnO and 0.86% ZnO slurries, thickening time results did not show marked differences in setting time. The difference may be attributed to the smaller amount of zinc used in this work and the lower solubility of ZnO (Chen et al. 2012) compared to the zinc salt used by Chamssine et al. (2022a). Also, calorimetry shows that the initial effect of zinc was to increase the heat release rate. Through ICP-MS, it is seen that the effect of zinc was to decrease the silicate concentration and to increase the aluminate content (see **Fig. 13**). It is possible that there was excess free silica in solution; therefore, the complexation with zincates and precipitation as C-S-H worked to capture this excess of silica and induced the dissolution of aluminates. Therefore, the dissolution stage of geopolymerization was enhanced rather than retarded, precipitating larger amounts of (C,K)-A-S-H and C-(K)-A-S-H, as seen in both SS **(Fig. 11)** and UCS **(Fig. 12)** results. Only later, the retardation effect can be observed as a slowing of the heat release rate, as seen in **Fig. 14.**

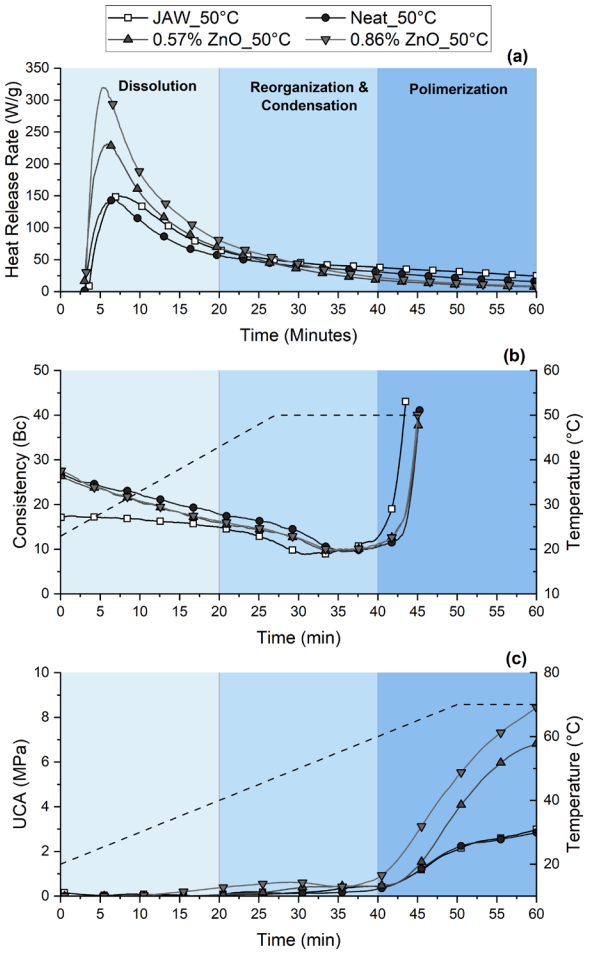

Fig. 14—Comparison between (a) heat release rate, (b) consistency profile, and (c) SS development, at the first hour after mixing, to understand the rock-based geopolymer kinetics.

From **Fig. 11** and **Table 12**, there was a small improvement from JAW (true one-part) to neat (formulation using KOH solution). Zinc addition, on the other hand, significantly improved the strength, with 0.86% ZnO paste giving the highest SS development up to 7 days, as well as the fastest setting and hardening times. Its SS is about three times that of the pure recipes JAW and neat. Omran and Khalifeh (2022) performed a wider study of the neat formulation, considering additional concentrations of zinc oxide and other additives, such as calcium oxide, calcium carbonate, and sodium hydroxide. Compared to those results, this work demonstrates that the new JAW formulation can reach strengths comparable to those of the neat one. The JAW formulation reaches a comparable strength after 1 day of curing, but the neat gains slightly less strength after 7 days. Formulations with zinc oxide suggest that the difference between 0.57% ZnO and 0.86% ZnO pastes becomes smaller after 7 days of curing, a result that was not seen in sonic strength curves. Higher concentrations did not increase the 1-day strength and therefore were not investigated in this work. However, the lack of retardation indicates that there is room to increase the ZnO content to increase the setting time.

Conclusions

Short-term chemical and mechanical properties of one-part geopolymer mixes were studied to obtain a better understanding of their geopolymerization mechanism for well-cementing applications. This investigation revealed some correlations between the chemical and mechanical properties of geopolymer cement. The addition of zinc oxide powder as a strength booster increases the rate of heat evolution and improves the early strength development. The higher the heat and energy evolution from geopolymerization reaction, the better the

early strength development. Moreover, the addition of zinc oxide powder does not have any effect on the slurry properties without any retardation.

Acknowledgments

The authors gratefully acknowledge TotalEnergies, AkerBP, ConocoPhillips, and Research Council of Norway for financially supporting the SafeRock KPN Project (RCN #319014319014— New Cementitious Material for Oil Well Cementing Applications—SafeRock) at the University of Stavanger, Norway. In addition, the authors would like to acknowledge Professor Oscar Reales and Dr. Paulo Moreira for thier collaboration.

References

Alvi, M. A. A., Khalifeh, M., and Agonafir, M. B. 2020. Effect of Nanoparticles on Properties of Geopolymers Designed for Well Cementing Applications. *J Pet Sci Eng* **191**. https://doi.org/10.1016/j.petrol.2020.107128.

Andrew, R. M. 2019. Global CO2 Emissions from Cement Production, 1928–2018. *Earth Syst Sci Data* **11**: 1675–1710. https://doi.org/10.5194/essd-11-1675-2019.

Anseau, M. R., Leung, J. P., Sahai, N. et al. 2005. Interactions of Silicate Ions with Zinc(II) and Aluminum(III) in Alkaline Aqueous Solution. *Inorg Chem* **44** (22): 8023–8032. https://doi.org/10.1021/ic050594c.

API RP 10B-2, *Recommended Practice for Testing Well Cements*. 2019. Washington, DC., USA: American Petroleum Institute.

ASTM C1365-18, *Standard Test Method for Determination of the Proportion of Phases in Portland Cement and Portland-Cement Clinker Using X-Ray Powder Diffraction Analysis*. 2018. West Conshohocken, Pennsylvania, USA: ASTM: .

ASTM C1702-17, *Standard Test Method for Measurement of Heat of Hydration of Hydraulic Cementitious Materials Using Isothermal Conduction Calorimetry*. 2017. West Conshohocken, Pennsylvania, USA: ASTM.

ASTM C597-16, *Standard Test Method for Pulse Velocity Through Concrete*. 2021. West Conshohocken, Pennsylvania, USA: ASTM.

ASTM D5673-16, *Standard Test Method for Elements in Water by Inductively Coupled Plasma—Mass Spectrometry*. 2016. West Conshohocken, Pennsylvania: ASTM.

ASTM E168-16, *Standard Practices for General Techniques of Infrared Quantitative Analysis*. 2016. West Conshohocken, Pennsylvania, USA: ASTM.

Barlet-Gouedard, V., Zusatz-Ayache, B., and Porcherie, O. 2008. Pumpable Geopolymer Formulation for Oilfield Application. 2008/017414 A1. WO.

Bergen, S. L., Zemberekci, L., and Nair, S. D. 2022. A Review of Conventional and Alternative Cementitious Materials for Geothermal Wells. *Renew Sust Energ Rev* **161**. https://doi.org/10.1016/j.rser.2022.112347.

Cai, J., Li, X., Tan, J. et al. 2020. Thermal and Compressive Behaviors of Fly Ash and Metakaolin-Based Geopolymer. *J Build Eng* **30**. https://doi.org/10.1016/j.jobe.2020.101307.

Chamssine, F., Khalifeh, M., and Saasen, A. 2022a. Rheological and Mechanical Properties of Rock-Based Geopolymers Developed for Well Abandonment: Effect of Chemical Admixtures at Elevated Temperatures. Paper presented at the ASME 2022 41st International Conference on Ocean, Offshore and Arctic Engineering, Hamburg, Germany, 5–10 June. https://doi.org/10.1115/OMAE2022-78376.

Chamssine, F., Khalifeh, M., Eid, E. et al. 2021. Effects of Temperature and Chemical Admixtures on the Properties of Rock-Based Geopolymers Designed for Zonal Isolation and Well Abandonment. Paper presented at the ASME 2021 40th International Conference on Ocean, Offshore and Arctic Engineering, Virtual, Online, 21–30 June. https://doi.org/10.1115/OMAE2021-60808.

Chamssine, F., Khalifeh, M., Saasen, A. et al. 2022b. Effect of Zn^{2+} and K^{+} as Retarding Agents on Rock-Based Geopolymers for Downhole Cementing Operations. *J Energy Resour Technol* **144** (5). https://doi.org/10.1115/1.4053710.

Chen, A., Xu, D., Chen, X. et al. 2012. Measurements of Zinc Oxide Solubility in Sodium Hydroxide Solution from 25 to 100 °C. *Trans Nonferrous Met Soc China* **22** (6): 1513–1516. https://doi.org/10.1016/S1003-6326(11)61349-6.

Damtoft, J. S., Lukasik, J., Herfort, D. et al. 2008. Sustainable Development and Climate Change Initiatives. *Cem Concr Res* **38**: 115–127. https://doi.org/10.1016/j.cemconres.2007.09.008.

Davidovits, J. 1991. Geopolymers: Inorganic Polymeric New Materials. *J Therm Anal* **37**: 1633–1656. https://doi.org/10.1007/BF01912193.

Davidovits, J. 2008. *Geopolymer: Chemistry & Applications*. Saint-Quentin, Paris: Institut Geopolymer.

Davidovits, J. 2013. *Geopolymer Cement a Review*, 1–11. Saint-Quentin, Paris: Institut Geopolymer.

Davidovits, J. 2017. Geopolymers: Ceramic-like Inorganic Polymers. *J Ceram Sci Technol* **8**: 335–350. https://doi.org/10.4416/JCST2017-00038.

Deshpande, A., Chiney, A., Patil, S. et al. 2015. Long-Term Study of Effects of CO2 Exposure on Cement Integrity Under Downhole Conditions. Paper presented at the EUROPEC 2015, Madrid, Spain, 1–4 June. SPE-174329-MS. https://doi.org/10.2118/174329-MS.

Falcone, J. S., Bass, J. L., Angelella, M. et al. 2010. The Determination of Sodium Silicate Composition Using ATR FT-IR. *Ind Eng Chem Res* **49** (14): 6287–6290. https://doi.org/10.1021/ie1002747.

Flatt, R. J., Roussel, N., and Cheeseman, C. R. 2012. Concrete: An Eco Material That Needs to Be Improved. *J Eur Ceram Soc* **32** (11): 2787–2798. https://doi.org/10.1016/j.jeurceramsoc.2011.11.012.

García-Lodeiro, I., Fernández-Jiménez, A., and Palomo, A. 2013. Variation in Hybrid Cements over Time. Alkaline Activation of Fly Ash–Portland Cement Blends. *Cem Concr Res* **52**: 112–122. https://doi.org/10.1016/j.cemconres.2013.03.022.

Garg, N. and White, C. E. 2017. Mechanism of Zinc Oxide Retardation in Alkali-Activated Materials: An in Situ X-Ray Pair Distribution Function Investigation. *J Mater Chem A* **5** (23): 11794–11804. https://doi.org/10.1039/C7TA00412E.

Gasteiger, H. A., Frederick, W. J., and Streisel, R. C. 1992. Solubility of Aluminosilicates in Alkaline Solutions and a Thermodynamic Equilibrium Model. *Ind Eng Chem Res* **31** (4): 1183–1190. https://doi.org/10.1021/ie00004a031.

Hewlett, P. C., ed. 2001. *Lea's Chemistry of Cement and Concrete*, fourth edition. Oxford, UK: Butterworth-Heinemann.

IEA2021. Net Zero by 2050 - A Roadmap for the Global Energy Sector.

Kamali, M., Khalifeh, M., and Saasen, A. 2022. Bonding Mechanism of Zonal Isolation Materials to Clean and Rusted Casing. *SPE J* **27** (5): 2613–2627. SPE-209812-PA. https://doi.org/10.2118/209812-PA.

Kamali, M., Khalifeh, M., Saasen, A. et al. 2020. Materials for Well Integrity: Characterization of Short-Term Mechanical Properties. Paper presented at the ASME 2020 39th International Conference on Ocean, Offshore and Arctic Engineering, Virtual, 3–7 August. https://doi.org/10.1115/OMAE2020-18623.

Khale, D. and Chaudhary, R. 2007. Mechanism of Geopolymerization and Factors Influencing Its Development: A Review. *J Mater Sci* **42** (3): 729–746. https://doi.org/10.1007/s10853-006-0401-4.

Khalifeh, M. and Saasen, A. 2020. *Introduction to Permanent Plug and Abandonment of Wells, Ocean Engineering & Oceanography*. Cham, Switzerland: Springer International Publishing. https://doi.org/10.1007/978-3-030-39970-2.

Khalifeh, M., Hodne, H., Saasen, A. et al. 2016a. Usability of Geopolymers for Oil Well Cementing Applications: Reaction Mechanisms, Pumpability, and Properties. Paper presented at the SPE Asia Pacific Oil & Gas Conference and Exhibition, Perth, Australia, 25–27 October. SPE-182354-MS. https://doi.org/10.2118/182354-MS.

Khalifeh, M., Motra, H. B., Saasen, A. et al. 2018. Potential Utilization for a Rock-Based Geopolymer in Oil Well Cementing. Paper presented at the ASME 2018 37th International Conference on Ocean, Offshore and Arctic Engineering, Madrid, Spain, 17–22 June. https://doi.org/10.1115/OMAE2018-78305.

Khalifeh, M., Saasen, A., Hodne, H. et al. 2019. Laboratory Evaluation of Rock-Based Geopolymers for Zonal Isolation and Permanent P&A Applications. *J Pet Sci Eng* **175**: 352–362. https://doi.org/10.1016/j.petrol.2018.12.065.

Khalifeh, M., Saasen, A., Vralstad, T. et al. 2014. Potential Utilization of Class C Fly Ash-Based Geopolymer in Oil Well Cementing Operations. *Cem Concr Compos* **53**: 10–17. https://doi.org/10.1016/j.cemconcomp.2014.06.014.

Khalifeh, M., Saasen, A., Vrålstad, T. et al. 2016b. Experimental Study on the Synthesis and Characterization of Aplite Rock-Based Geopolymers. *J Sustain Cem-Based Mater* **5** (4): 233–246. https://doi.org/10.1080/21650373.2015.1044049.

Khalifeh, M., Todorovic, J., Vrålstad, T. et al. 2017. Long-Term Durability of Rock-Based Geopolymers Aged at Downhole Conditions for Oil Well Cementing Operations. *J Sustain Cem-Based Mater* **6** (4): 217–230. https://doi.org/10.1080/21650373.2016.1196466.

Kiran, R., Teodoriu, C., Dadmohammadi, Y. et al. 2017. Identification and Evaluation of Well Integrity and Causes of Failure of Well Integrity Barriers (A Review). *J Nat Gas Eng* **45**: 511–526. https://doi.org/10.1016/j.jngse.2017.05.009.

Krishna, R. S., Mishra, J., Zribi, M. et al. 2021. A Review on Developments of Environmentally Friendly Geopolymer Technology. *Mater* **20**. https://doi.org/10.1016/j.mtla.2021.101212.

Kumar, S., Kumar, R., and Mehrotra, S. P. 2010. Influence of Granulated Blast Furnace Slag on the Reaction, Structure and Properties of Fly Ash Based Geopolymer. *J Mater Sci* **45** (3): 607–615. https://doi.org/10.1007/s10853-009-3934-5.

Luukkonen, T., Abdollahnejad, Z., Yliniemi, J. et al. 2018. One-Part Alkali-Activated Materials: A Review. *Cem Concr Res* **103**: 21–34. https://doi.org/10.1016/j.cemconres.2017.10.001.

Mahmoudkhani, A. H., Huynh, D. N. T., Sylvestre, C. et al. 2008. New Environment-Friendly Cement Slurries With Enhanced Mechanical Properties. Paper presented at the CIPC/SPE Gas Technology Symposium 2008 Joint Conference, Calgary, Alberta, Canada, 16–19 June. SPE-115004-MS. https://doi.org/10.2118/115004-MS.

Matalkah, F., Xu, L., Wu, W. et al. 2017. Mechanochemical Synthesis of One-Part Alkali Aluminosilicate Hydraulic Cement. *Mater Struct* **50** (1). https://doi.org/10.1617/s11527-016-0968-4.

McLellan, B. C., Williams, R. P., Lay, J. et al. 2011. Costs and Carbon Emissions for Geopolymer Pastes in Comparison to Ordinary Portland Cement. *J Clean Prod* **19** (9–10): 1080–1090. https://doi.org/10.1016/j.jclepro.2011.02.010.

Myers, R. J., Bernal, S. A., and Provis, J. L. 2014. A Thermodynamic Model for C-(N-)A-S-H Gel: CNASH-Ss. *Cem Concr Res* **66**: 27–47. https://doi.org/10.1016/j.cemconres.2014.07.005.

Nasvi, M. C. M., Ranjith, P. G., and Sanjayan, J. 2014a. Effect of Different Mix Compositions on Apparent Carbon Dioxide (CO2) Permeability of Geopolymer: Suitability as Well Cement for CO2 Sequestration Wells. *Appl Energy* **114**: 939–948. https://doi.org/10.1016/j.apenergy.2013.05.050.

Nasvi, M. C. M., Ranjith, P. G., Sanjayan, J. et al. 2014b. A Numerical Study of CO2 Flow through Geopolymer under Down-Hole Stress Conditions: Application for CO2 Sequestration Wells. *J Unconv Oil Gas Resour* **7**: 62–70. https://doi.org/10.1016/j.juogr.2014.01.002.

Nasvi, M. C. M., Ranjith, P. G., Sanjayan, J. et al. 2014c. Effect of Temperature on Permeability of Geopolymer: A Primary Well Sealant for Carbon Capture and Storage Wells. *Fuel* **117**: 354–363. https://doi.org/10.1016/j.fuel.2013.09.007.

Nasvi, M. C. M., Ranjith, P. G., Sanjayan, J. et al. 2014d. Mechanical Behaviour of Wellbore Materials Saturated in Brine Water with Different Salinity Levels. *Energy* **66**: 239–249. https://doi.org/10.1016/j.energy.2013.12.003.

Nedunuri, A. S. S. S. and Muhammad, S. 2022. The Role of Zinc Sulphate as a Retarder for Alkali Activated Binders and Its Influence on the Rheological, Setting and Mechanical Behaviour. *Constr Build Mater* **344**. https://doi.org/10.1016/j.conbuildmat.2022.128128.

Nelson, E. B. and Guillot, D., eds. 2006. *Well Cementing*, second edition. Houston, Texas, USA: Schlumberger.

Nematollahi, B. and Sanjayan, J. 2014. Effect of Different Superplasticizers and Activator Combinations on Workability and Strength of Fly Ash Based Geopolymer. *Mater & Des* **57**: 667–672. https://doi.org/10.1016/j.matdes.2014.01.064.

Omran, M. and Khalifeh, M. 2022. Development of Low Carbon Dioxide Intensive Rock-Based Geopolymers for Well Cementing Applications – One-Part Geopolymer, in: Volume 10: Petroleum Technology. Paper presented at the ASME 2022 41st International Conference on Ocean, Offshore and Arctic Engineering, Hamburg, Germany, 5–10 June. https://doi.org/10.1115/OMAE2022-78535.

Omran, M. and Khalifeh, M. 2023. Development of One-Part Rock-Based Geopolymers for Downhole Cementing Applications. *J Energy Resour Technol* **145** (10): 10. https://doi.org/10.1115/1.4062250.

Omran, M., Khalifeh, M., and Hjelm, S. 2022a. Role of Zeta Potential on Rheology of One-Part Geopolymer Slurries: Influence of Superplasticizers. In *Annual Transactions of the Nordic Rheology Society*, Vol. 30. Aarhus, Denmark: Nordic Rheology Society.

Omran, M., Khalifeh, M., and Saasen, A. 2022b. Influence of Activators and Admixtures on Rheology of Geopolymer Slurries for Well Cementing Applications. Paper presented at the SPE Asia Pacific Oil & Gas Conference and Exhibition, Adelaide, Australia, 17–19 October. SPE-210698-MS. https://doi.org/10.2118/210698-MS.

Omran, M., Hjelm, S., Khalifeh, M. et al. 2023. Synthesis of Sustainable One-Part Geopolymers for Well Cementing Applications. *Geoenergy Sci Eng* **227**. https://doi.org/10.1016/j.geoen.2023.211822.

Pacheco-Torgal, F., Castro-Gomes, J., and Jalali, S. 2008. Alkali-Activated Binders: A Review. *Constr Build Mater* **22** (7): 1305–1314. https://doi.org/10.1016/j.conbuildmat.2007.10.015.

Pacheco-Torgal, F., Labrincha, J., Leonelli, C. et al., eds. 2014. *Handbook of Alkali-Activated Cements, Mortars and Concretes*. Sawston, UK: Woodhead Publishing.

Paiva, M. D. M., Fonseca Rocha, L. D., Castrillon Fernandez, L. I. et al. 2021. Rheological Properties of Metakaolin-Based Geopolymers for Three-Dimensional Printing of Structures. *ACI Mater J* **118** (6). https://doi.org/10.14359/51733122.

Paiva, M. D. M., Silva, E. C. C. M., Melo, D. M. A. et al. 2018. A Geopolymer Cementing System for Oil Wells Subject to Steam Injection. *J Pet Sci Eng* **169**: 748–759. https://doi.org/10.1016/j.petrol.2018.06.022.

Palacios, M. and Puertas, F. 2005. Effect of Superplasticizer and Shrinkage-Reducing Admixtures on Alkali-Activated Slag Pastes and Mortars. *Cem Concr Res* **35**: 1358–1367. https://doi.org/10.1016/j.cemconres.2004.10.014.

Palomo, A., Krivenko, P., Garcia-Lodeiro, I. et al. 2014. A Review on Alkaline Activation: New Analytical Perspectives. *Mater Constr* **64**. https://doi.org/10.3989/mc.2014.00314.

Salehi, S., Khattak, M. J., Ali, N. et al. 2018. Study and Use of Geopolymer Mixtures for Oil and Gas Well Cementing Applications. *J Energy Resour Technol* **140** (1): 1–12. https://doi.org/10.1115/1.4037713.

Salehi, S., Khattak, M. J., Bwala, A. H. et al. 2017. Characterization, Morphology and Shear Bond Strength Analysis of Geopolymers: Implications for Oil and Gas Well Cementing Applications. *J Nat Gas Sci Eng* **38**: 323–332. https://doi.org/10.1016/j.jngse.2016.12.042.

Salehi, S., Khattak, J., Saleh, F. K. et al. 2019. Investigation of Mix Design and Properties of Geopolymers for Application as Wellbore Cement. *J Pet Sci Eng* **178**: 133–139. https://doi.org/10.1016/j.petrol.2019.03.031.

Simao, C. A., Folsta, M. G., Campos, G. et al. 2016. Cementing Solutions for Salt- and CO2-Laden Presalt Zones. Paper presented at the SPE Deepwater Drilling and Completions Conference, Galveston, Texas, USA, 14–15 September. SPE-180336-MS. https://doi.org/10.2118/180336-MS.

Singh, N. B. and Middendorf, B. 2020. Geopolymers as an Alternative to Portland Cement: An Overview. *Constr Build Mater* **237**. https://doi.org/10.1016/j.conbuildmat.2019.117455.

Sturm, P., Gluth, G. J. G., Brouwers, H. J. H. et al. 2016. Synthesizing One-Part Geopolymers from Rice Husk Ash. *Constr Build Mater* **124**: 961–966. https://doi.org/10.1016/j.conbuildmat.2016.08.017.

Suwan, T. and Fan, M. 2017. Effect of Manufacturing Process on the Mechanisms and Mechanical Properties of Fly Ash-Based Geopolymer in Ambient Curing Temperature. *Mater Manuf Process* **32**: 461–467. https://doi.org/10.1080/10426914.2016.1198013.

Taylor, H. F. W. 1997. *Cement Chemistry*, second edition. London, England: Thomas Telford Publishing. https://doi.org/10.1680/cc.25929.

Tommaseo, C. E. and Kersten, M. 2002. Aqueous Solubility Diagrams for Cementitious Waste Stabilization Systems. 3. Mechanism of Zinc Immobilizaton by Calcium Silicate Hydrate. *Environ Sci Technol* **36**: 2919–2925. https://doi.org/10.1021/es0102484.

Wan-En, O., Yun-Ming, L., Cheng-Yong, H. et al. 2022. Towards Greener One-Part Geopolymers through Solid Sodium Activators Modification. *J Clean Prod* **378**. https://doi.org/10.1016/j.jclepro.2022.134370.

Wang, L., Geddes, D. A., Walkley, B. et al. 2020. The Role of Zinc in Metakaolin-Based Geopolymers. *Cem Concr Res* **136**. https://doi.org/10.1016/j.cemconres.2020.106194.

Yao, X., Zhang, Z., Zhu, H. et al. 2009. Geopolymerization Process of Alkali–Metakaolinite Characterized by Isothermal Calorimetry. *Thermochim Acta* **493** (1–2): 49–54. https://doi.org/10.1016/j.tca.2009.04.002.

Zailan, S. N., Bouaissi, A., Mahmed, N. et al. 2020. Influence of ZnO Nanoparticles on Mechanical Properties and Photocatalytic Activity of Self-Cleaning ZnO-Based Geopolymer Paste. *J Inorg Organomet Polym* **30** (6): 2007–2016. https://doi.org/10.1007/s10904-019-01399-3.

Zhang, Z., Provis, J. L., Wang, H. et al. 2013. Quantitative Kinetic and Structural Analysis of Geopolymers. Part 2. Thermodynamics of Sodium Silicate Activation of Metakaolin. *Thermochim Acta* **565**: 163–171. https://doi.org/10.1016/j.tca.2013.01.040.

Zhang, Z., Wang, H., Provis, J. L. et al. 2012. Quantitative Kinetic and Structural Analysis of Geopolymers. Part 1. The Activation of Metakaolin with Sodium Hydroxide. *Thermochim Acta* **539**: 23–33. https://doi.org/10.1016/j.tca.2012.03.021.